Comparing flux-averaged and resident concentration in a fractured bedrock using ground penetrating radar

Matthew W. Becker[1] and Georgios P. Tsoflias[2]

Received 1 June 2009; revised 18 February 2010; accepted 29 April 2010; published 15 September 2010.

[1] Saline tracer transport experiments were performed to compare flux-averaged and resident concentration in a single subhorizontal fracture in sandstone bedrock. Tracer migration over a 14 m distance was monitored at an extraction well and imaged within the rock as it passed below a ground penetrating radar (GPR) positioned at the surface. Reflected radar amplitude was calibrated to tracer concentration by circulating saline fluid of known concentration through the fracture. Saline breakthrough curves measured at the well and within the rock were comparable but showed differences in both magnitude and shape. Transport differences were explored using flux-averaged and resident concentration first-passage-time models combined with streamline advective tracking. Application of the appropriate transport model to the two breakthrough curves produced identical estimates of dispersivity and similar estimates of effective fracture aperture. The tracer-derived fracture aperture also agreed reasonably well with hydraulic aperture derived from cross-hole pump tests. The availability of both flux and resident concentrations helped constrain the interpretation of the flow and transport behavior in the fracture. Flow appeared to be highly channelized with less than half the hydraulically swept area of the fracture contributing to efficient tracer transport.

Citation: Becker, M. W., and G. P. Tsoflias (2010), Comparing flux-averaged and resident concentration in a fractured bedrock using ground penetrating radar, *Water Resour. Res.*, *46*, W09518, doi:10.1029/2009WR008260.

1. Introduction

[2] Recent advancements in geophysical imaging of hydrologic systems (hydrogeophysics) require a reassessment of some standard concepts in transport phenomena. The interpretation of groundwater tracer tests, for example, is traditionally based upon the assumption that water will be pumped at a point for analysis, implying that measured concentrations are flux-averaged (i.e., the mass rate divided by the flow rate). Hydrogeophysical methods are capable of interrogating a volume of the subsurface in situ, however, implying a volume-averaged (resident) concentration (i.e., the mass in the sample divide by the volume of the sample). As a consequence, different theoretical transport models may be required in order to interpret concentrations derived from tracer tests and concentrations inverted from hydrogeophysical imaging. The choice of transport models can have important implications for monitoring and understanding transport in groundwater.

[3] When the ratio of characteristic transport length to hydrodynamic dispersion is high (large Peclet numbers), flux-averaged and resident concentrations produce similar estimations of solute movement [*Kreft and Zuber*, 1978]. In highly dispersive transport systems, however, the difference between flux-averaged and resident concentrations can become significant. One of the most dispersive systems encountered in groundwater investigations is fractured bedrock, where groundwater velocities can vary orders of magnitude over submeter distances. The variation in groundwater velocity results in the channelization of flow through fractures and fracture networks. In such systems, tracer tests that produce flux-averaged concentrations may not be directly applicable to reactive models that generally require volume-averaged concentration.

[4] Here we present experiments that elucidate the contrast between flux-averaged and resident concentrations in fractured bedrock, and we discuss the advantage of the integration of the two methods. A saline tracer test was conducted in a single bedding plane fracture. Flux-averaged concentrations were measured using water sampled from a pumped well, and resident concentrations were measured remotely by changes in the amplitude of reflected ground penetrating radar (GPR) signals. The meaning of tracer breakthrough in the context of pumped sampling and GPR reflection imaging is explored here. We test the hypothesis that flux-averaged concentrations should be used for tracer breakthrough measured at an extraction well and resident concentrations should be used for breakthrough measured at the surface by GPR reflections. New analytic tools are presented that support the testing of this hypothesis and the appropriate treatment of tracer breakthrough measured at pumping wells and through a subsurface control volume.

2. Background

[5] The distinction between flux-averaged and resident concentrations was first recognized by chemical engineers [*Aris*, 1956; *Dankwerts*, 1953] and later adopted by tracer

[1]California State University, Long Beach, California, USA.
[2]University of Kansas, Lawrence, Kansas, USA.

0043-1397/10/2009WR008260

hydrologists [*Kreft and Zuber*, 1978]. Early research focused on dispersion phenomena in homogenous systems and was later adopted for stochastic groundwater hydrology [*Shapiro and Cvetkovic*, 1988]. While the difference between flux-averaged and resident concentration has been well documented in laboratory column tests, however, discussion regarding field behavior has been largely theoretical. It is only with the recent advances in geophysical imaging techniques that it has become feasible to extract resident concentrations from field experiments [*Hubbard and Rubin*, 2000].

[6] Because the difference in flux-averaged and resident concentrations is expected to be significant only in highly dispersive systems, we examine the issue using the example of flow and transport in fractured bedrock. The heterogeneity of permeability in bedrock is typically large. Even in single fractures, contrasts in permeability may be so severe that water flows in a channeled manner, preferentially moving through larger apertures [*Tsang and Neretnieks*, 1998]. Flow channels develop naturally in response to a forced hydraulic gradient and will take on a different character in response to different hydraulic stresses. The local variation in velocity can be sufficiently large that relatively slow advection in small apertures can manifest itself as a diffusion-like process in tracer breakthrough curves [*Becker and Shapiro*, 2000; *Becker and Shapiro*, 2003; *Liu et al.*, 2007; *Shapiro*, 2001; *Zhou et al.*, 2007].

[7] In spite of the fact that flow channeling has been observed at wells and seepage faces for decades [*Bourke*, 1987; *Moreno et al.*, 1985; *Neretnieks et al.*, 1982; *Neretnieks*, 1983; *Neretnieks*, 1987], there is still a poor understanding of how channeling appears in situ. One example in which channeled transport was monitored in situ was conducted by *Day-Lewis et al.* [2003, 2006] at the fracture granite/schist of the Mirror Lake Site. Time-lapse borehole radar tomography showed that tracer moved in a channeled manner, with some of the saline fluid likely taking a circuitous route between the injection-extraction wells that passed outside the region of radar imaging.

[8] Surface reflection GPR surveying has been used successfully to image fractures [*Davis and Annan*, 1989; *Grasmueck*, 1996; *Seol et al.*, 2001], and its potential to determine important fracture hydraulic properties is the subject of ongoing investigations. *Lane et al.* [2000] evaluated GPR signal changes for the detection of free-phase hydrocarbons in discrete fractures. *Tsoflias et al.* [2001] used time lapse imaging to monitor drainage of a shallow fracture during a pumping test. *Tsoflias* [2008] employed surface 3-D GPR imaging and fracture reflection amplitude to map aperture variability along the fracture surface and flow conduit connectivity that was in agreement with tracer tests conducted by earlier investigators [*Muldoon and Bradbury*, 2005]. *Gregoire et al.* [2003] and *Gregoire and Hollender* [2004] exploited the amplitude response of reflected radar signals in an inverse scheme to determine apertures of air filled fractures in a salt mine and in controlled experiments using granite blocks. *Gregoire et al.* [2006] used reflection borehole radar to monitor steam injection in a fractured limestone bedrock and investigated changes in electromagnetic (EM) wave amplitude and velocity of propagation to change in interstitial water temperature, displacement of matrix pore water and fracture fluid by steam, and to increased electrical conductivity related to matrix and fluid temperature rise.

[9] The work presented here builds upon previous GPR imaging of saline tracer transport conducted at the Altona research site in Northeastern New York State, USA. In one series of experiments, tracer was circulated between two wells in a subhorizontal bedrock fracture while GPR antennae were moved in a grid pattern along the surface [*Talley*, 2005; *Talley et al.*, 2005]. The difference between posttracer and pretracer reflection amplitudes indicated the spatial distribution of tracer in the fracture plane [*Talley et al.*, 2005]. These experiments showed that saline tracer moves in a highly heterogeneous manner in a single rock fracture, apparently in the absence of guiding features such as intersecting fractures.

[10] In subsequent investigations at Altona, *Tsoflias and Becker* [2008] used analytical modeling, numerical simulations, and field experiments to examine surface GPR reflection amplitude and phase response to fractures saturated with water of varying salinity. They concluded that GPR signal responses are characteristic and quantifiable and, therefore, can be related to fracture aperture and fluid salinity for hydrologic investigations of fractured rock flow and transport properties.

[11] In the experiments reported here, as in *Tsoflias and Becker* [2008], radar antennae are held in a single position while water of varying salinity is circulated through the underlying fracture. Thus, the saline tracer is imaged through time rather than through space. We will show that GPR-measured tracer breakthrough is comparable but not equivalent to tracer breakthrough measured at a monitoring well. We discuss the implications of this comparison for transport in fractured bedrock.

3. Methods

3.1. Field Site

[12] Field experiments were performed at the Altona Flat Rock site, located approximately 15 km northwest of Plattsburgh, NY, USA. Altona Flat Rock is part of a large system of Cambrian Potsdam Sandstone (well-sorted quartzose) pavements that were stripped of overburden during the last glaciation and remain exposed today [*Rayburn et al.*, 2005]. There are laterally extensive subhorizontal (dipping ~3°) bedding plane partitions that are visible in numerous outcrops surrounding the site. Because the sandstone is highly cemented with silica, primary porosity is insignificant in comparison to secondary porosity. Extensive tracer experiments have been conducted among five 15 cm diameter open-hole wells arranged in a five-spot configuration with 10 m on a side (Figure 1, inset). The wells intersect a major subhorizontal fracture 7.6 m below ground surface that has been the focus of those investigations. The thin overburden has been cleared in this area to present a clean sandstone pavement for GPR imaging of the 7.6 m fracture. The Altona Flat Rock site is part of the William H. Miner Agricultural Research Institute that has granted us permission to develop the site and has provided us with logistical support.

3.2. Tracer Experiments

[13] Controlled dipole (recirculation) tracer tests were conducted between wells 204 and 304 (Figure 1, inset). Table salt was used as a tracer and monitored using GPR

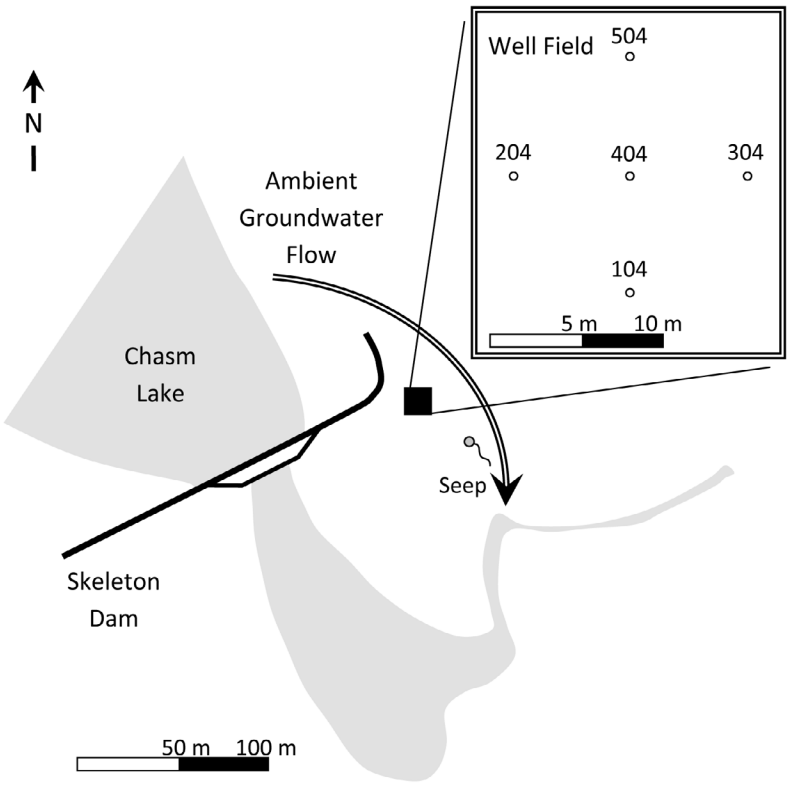

Figure 1. Altona Flat Rock site and the well field (inset) in which tracer experiments were conducted.

reflection from surface. Salt behaves conservatively in this system as demonstrated by many previous saline tracer tests in which formation water quickly returns to background electrical conductivity upon pumping [*Talley*, 2005; *Talley et al.*, 2005]. Before tracer injection, water was pumped from well 304 at a rate of 3 L/min and reinjected in well 204 until steady heads were registered at all wells. Pumping was accomplished with a variable speed pump (Grundfos RediFlo-2) placed at the depth of the fracture. The fracture was isolated in both wells by the water level approximately 1 m above the fracture and by inflatable packers approximately 0.5 m below the fracture. Packers constructed entirely of plastic (RockTest) were used to reduce disturbance to the radar. Recirculation of the water created pseudo steady state full-dipole flow field superimposed over the natural flow field. The background hydraulic gradient decreases from Chasm Lake to seeps at the edge of the outcrop (Figure 1) and was measured to be 0.0037 before pumping using e-tapes referenced to a laser-level datum. On the basis of an average transmissivity of 5 m^2/d estimated from cross-hole pumping tests [*Talley et al.*, 2005], this gradient suggests an ambient specific discharge of 26 m/d to the southeast.

[14] Reinjected water passed through a 20 L tank at the surface near well 204 to provide a means of measuring tracer concentration and assuring full mixing of the salt (Figure 2). Tracer concentration was measured in the surface tank by recording electrical conductivity with a digital electrical conductivity probe (Orion) and then converting it to mass concentration using a calibration curve prepared on site using gravimetric measurements of salt. The tracer experiment was initiated by adding 1 kg of salt to the surface tank and stirring vigorously. The volume of fluid in the tank was 8 L so the initial concentration was 125 g/L. Conductivity was also monitored using a probe in the injection interval of well 204 (Levelogger TLC, Solinst). Unfortunately, this probe and a second probe in the surface tank, both failed during GPR data collection. Concentration measurements at the well collected later in the day were,

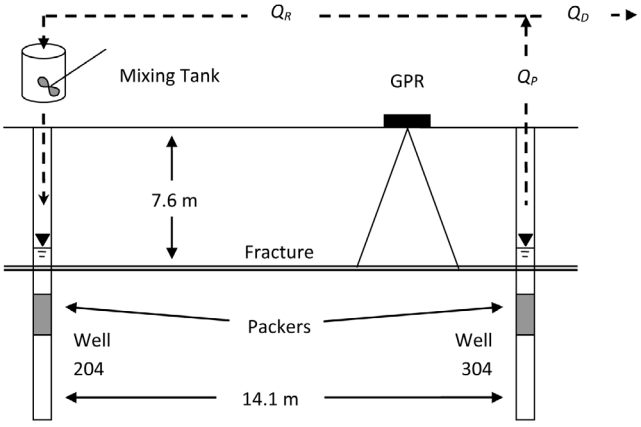

Figure 2. Cross-sectional schematic of the tracer experiment. Water from well 304 was reinjected into well 204 to create recirculation. Salt was added into the surface mixing tank. Discharge rates for pumping, reinjection, and discharge are denoted as Q_P, Q_R, and Q_D, respectively. Drawing not to scale.

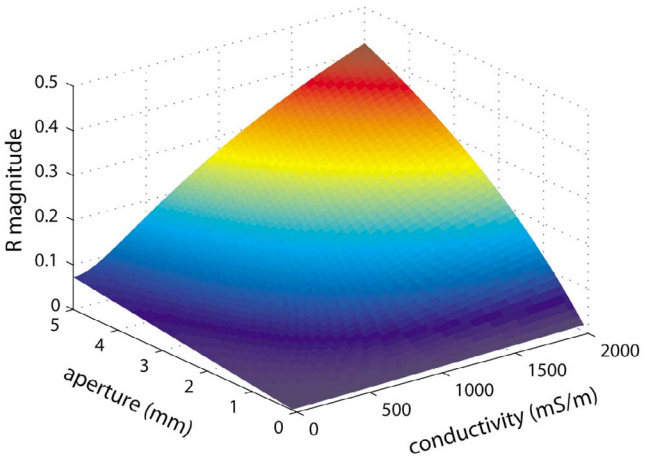

Figure 3. Theoretical relationship among reflection magnitude, fracture aperture, and water electrical conductivity for a 50 MHz frequency signal.

therefore, used to compare to the GPR results. The later test was identical to the test monitored with radar, except water was recirculated at a slightly slower rate (2.8 L/min instead of 3 L/min) and more salt was injected (1463 g instead of 1000 g). Available data before the surface probe failure indicate that the test was entirely repeatable so long as the concentration and breakthrough time were normalized to the injected mass and recirculation rate, respectively.

3.3. GPR Imaging

[15] Previous GPR work at Altona [*Talley et al.*, 2005; *Tsoflias and Becker*, 2008] has shown that saline tracer in the 7.6 m depth fracture can be imaged from the surface using reflected GPR signal amplitude changes. An important finding of the earlier work is that lower frequency GPR is more sensitive to changes in fluid electrical conductivity than higher frequency. Therefore, we used 50 MHz GPR to monitor saline tracer breakthrough in the 7.6 m fracture. Figure 3 shows the theoretical reflection coefficient magnitude (R) of a 50 MHz frequency signal as a function of fracture aperture (0–5 mm) and water electrical conductivity (0–2000 mS/m). The model employs the recursive method used in plane-wave studies that considers field continuity and matches the impedances across planar interfaces to compute complex reflection and transmission coefficients [*Balanis*, 1989]. To simulate field conditions, the model considers a parallel polarized wavefield impinging at 7.5° to the fracture surface; rock matrix relative permittivity and electrical conductivity of 7 and 0.1 mS/m, respectively; and water relative permittivity of 80.

[16] The analytically computed reflection coefficient magnitude R (R can reach a theoretical maximum magnitude of 1.0) suggests that saline tracer breakthrough of up to 2 S/m will result in significant change in the reflectivity of a millimeter-scale aperture fracture. However, in this theoretical analysis, fracture aperture is assumed to be constant (i.e., parallel plate aperture) over the ~2.9 m radius Fresnel zone illuminated by the GPR wavefield. In reality, aperture and conductivity both vary in space, and these spatial distributions are likely to be highly correlated because larger apertures tend to conduct traced fluid. In addition, the analytical reflection coefficient model does not account for wave propagation effects, such as signal attenuation and dispersion. Although the theoretical GPR model does not capture all the subtle complexities of the field data, it offers valuable insight about the expected response of GPR amplitude to tracer breakthrough at Altona. Because of the expected simplified representation of subsurface conditions by the theoretical model, we have chosen to use an empirical field calibration approach to quantitatively relate observed GPR reflection amplitude to fracture water electrical conductivity.

[17] To calibrate the change in GPR reflection amplitude with fluid conductivity in the fracture, we conducted a series of tracer recirculation experiments between the injection well 204 and the pumping well 304, while radar antennae remained stationary at the same location shown in Figure 4. Stationary antennae ensured constant fracture geometry and rock matrix effects to the propagating wavefield and allowed direct observation of GPR signal changes related to fluid electrical conductivity changes. In these experiments, fluid conductivity in the fracture was increased in a stepwise fashion, whereas radar imaging was conducted over time. Injection in well 404, 3.6 m up-gradient from the radar antennae, was selected to provide better control of saline tracer concentration circulated below the antennae.

[18] The calibration procedure was to initialize a near steady state head condition by circulating water as described for the tracer experiments. Tracer was introduced and allowed

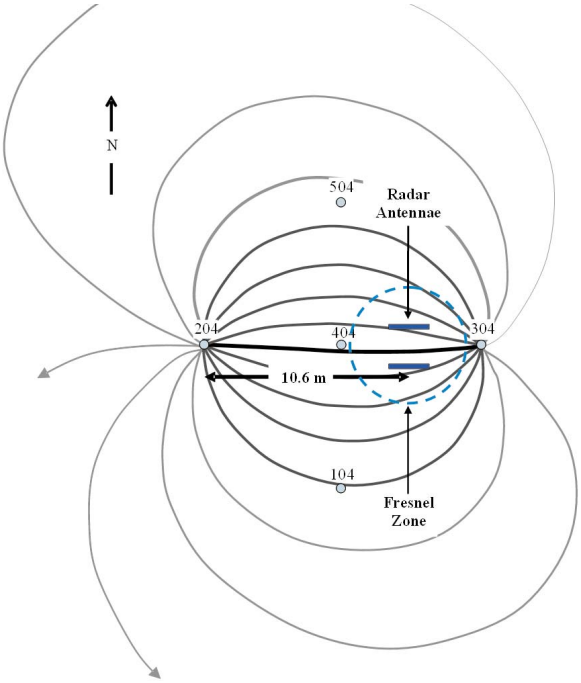

Figure 4. Map view schematic of tracer experiments showing position of radar antennae and approximate Fresnel zone. Idealized streamlines showing flow from injection well 204 to extraction well 304, assuming a background uniform flow to the SE. The central predicted pathways are shown in darker gray and the most direct pathway is shown in black.

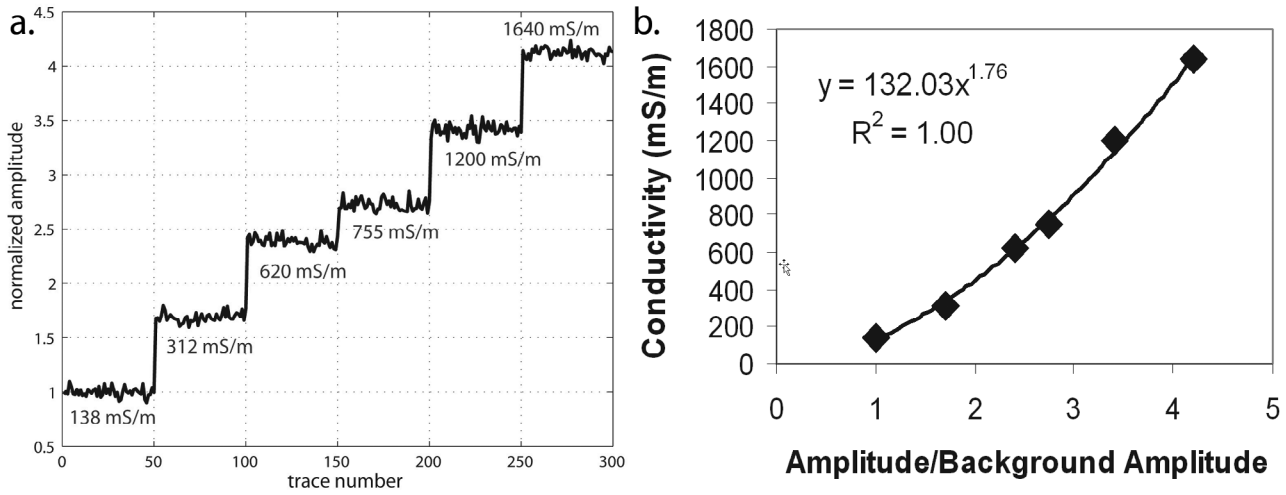

Figure 5. Calibration tracer experiment relating reflected GPR amplitude normalized to pretracer reflected amplitude. (a) Normalized amplitude versus trace number that corresponds to step-elevated concentrations measured at the extraction well. (b) Corresponding empirical relationship between normalized amplitude and electrical conductivity.

to reach a steady value that was assumed to represent "saturation" of the fracture with the saline tracer, i.e., nearly complete mixing of saline fluid through the recirculated area of the fracture and the boreholes. Because some of the recirculated water is lost to the background natural flow field, the electrical conductivity of pumped and reinjected water declined slightly through time within each injection step, so an average amplitude and concentration were compared at each steady portion of the step. Fifty GPR traces were acquired at each one of the six "saturation" conditions ranging from 138 to 1640 mS/m. Figure 5a shows a plot of GPR fracture reflection amplitude normalized to the average background reflection corresponding to water electrical conductivity of 138 mS/m. A stepwise increase of recorded GPR amplitudes in response to the stepwise increase of fracture saline fluid saturation is evident.

[19] By comparing the steady electrical conductivity in the recirculated water and normalized GPR amplitude (post-tracer maximum reflection amplitude divided by average pretracer maximum reflection amplitude) for each injection step, a location specific conductivity versus amplitude calibration relationship was developed (Figure 5b). A power law function was fit by regression through the data that adequately represented ($R^2 = 0.997$) the relationship between conductivity in the recirculated fluid and normalized amplitude. The calibration relationship exhibits the expected trend as predicted by the analytical model in Figure 3 and published work by *Tsoflias and Becker* [2008]. This function was used to convert reflected amplitudes registered at the radar to conductivity in the pumped water. A calibration of electrical conductivity measured with the conductivity meter to standard dilutions of the table salt was used to relate conductivity to mass concentrations. Thus, normalized reflected amplitudes observed with the GPR system at the fracture location shown in Figure 2 could be related to mass concentrations in the circulated water.

[20] It is important to note that the electrical conductivity measured at the pumping well is not necessarily the electrical conductivity of fluid detected by the radar. Flow is highly heterogeneous, and the entire fracture may not be flooded by fluid of uniform salinity. The recorded GPR amplitude is the response to both fresh and saline water contained in the Fresnel zone, whereas the pumped well measures only the flowing saline water. As a consequence, the calibration performed to relate radar amplitude to fluid electrical conductivity (Figure 5b) is site specific and it incorporates a greater level of complexity than predicted by the theoretical parallel plate, uniform saturation model illustrated in Figure 3.

3.4. Transport Modeling

[21] An objective of this work was to compare tracer transport measured at a pumping well and within the rock by the radar. As discussed in the introduction, these two measurements represent flux- and volume-averaged (resident) concentrations [*Kreft and Zuber*, 1978]. Here we model transport using a one-dimensional first-passage-time description of transport, which is the flux of mass across a stationary boundary [*Becker and Charbeneau*, 2000]. In Laplace space, the advection-dispersion transfer function is

$$\overline{F}_t(s) = \exp\left[\frac{Pe}{2}\left(1 - \sqrt{1 + \frac{4\tau s}{Pe}}\right)\right], \qquad (1)$$

where Pe is the Peclet number, τ is the mean residence time of the particle in the system, and s is the Laplace variable of integration. The Peclet number is x/α_L, where α_L is the longitudinal dispersivity and x is a characteristic length. For one-dimensional uniform flow, x may be interpreted to be the length of a theoretical "column" through which the mass moves [*Becker and Charbeneau*, 2000]. Thus, this representation of transport includes only advection and dispersion tangential to the fluid velocity.

[22] This solution is mathematically equivalent to the solution of the one-dimensional advection-dispersion equation with a Dirac inlet condition and an infinite outlet condition. It is used here as a transfer function for the

formation, thereby allowing recirculation to be readily modeled. *Becker and Charbeneau* [2000] discuss how the first-passage-time solution is necessary to correctly account for mass balance when multiple transfer functions are placed in series.

[23] Flow between the injection and pumping wells is characterized by diverging and converging streamlines and varying water velocity along each streamline (e.g., Figure 4). Multiple streamlines are easily represented using transfer functions by apportioning equally the injected tracer mass along a finite number of streamlines and summing the breakthrough over time. Equation (1), however, requires constant velocity along the transport pathway, whereas recirculation between injection and pumping wells implies varying velocity. Variable velocity is handled here by partitioning the transport pathway into segments of constant velocity. Each segment is represented by equation 1 using the appropriate resident time, τ. Many transfer functions are placed in series to represent the varying velocity along the streamline. Residence time of each segment is calculated using a Runga-Kutta particle tracking formulation, based upon a velocity field calculated using an analytic element solution of the flow equation [*Rabideau et al.*, 2007]. There is little computational cost in using multiple streamlines or transfer functions within streamlines because all calculations are performed in Laplace space. In Laplace space, accounting of multiple streamlines is computed through summation of transfer functions and convolution is computed through the multiplication of transfer functions. After algebraic manipulation, the entire transport solution is numerical inverted only once to the time domain. This is accomplished with a fast Fourier transform reformulated for one-sided Laplace transforms [*Becker and Charbeneau*, 2000]. Readers are referred to the article by *Becker and Jiang* [2007] for a full discussion of technique.

[24] There is likely to be some error in this streamline solution because of the effect of cross-flow as the dipole is superimposed over the background uniform flow [*Stephenson and Novakowski*, 2006]. For the purposes of analyzing these tracer breakthrough data, however, this streamline approach allows for efficient computation of the transport that allows nonlinear regression data fitting with minimal computer run times. It also simplified comparison of flux-averaged and resident concentrations by removing the effect of numerical errors from the problem.

[25] In addition to transport through the formation, we must account for residence time in the mixing tank at the surface and boreholes and the recirculation of mass because of reinjection of traced fluid. Residence time in the mixing tanks are accounted for using an algebraic function in Laplace space (see appendix in *Becker and Shapiro* [2000] for a discussion):

$$\overline{C}_{\mathrm{F}}(s) = M_0\left(\frac{\overline{F}_{\mathrm{S}}\overline{F}_{\mathrm{F}}}{1-\rho\overline{F}_{\mathrm{S}}\overline{F}_{\mathrm{F}}}\right), \tag{2}$$

where $\overline{C}_{\mathrm{F}}$ is the flux-averaged concentration in the recirculated system, $\overline{F}_{\mathrm{S}}$ is the transfer function of the source term, $\overline{F}_{\mathrm{F}}$ is the transfer function that represents transport in the formation from the injection well to the pumping well, and M_0 is the injected mass. The parameter ρ is the ratio of discharge that is reinjected to the total discharge pumped from the well ($\rho = Q_{\mathrm{R}}/Q_{\mathrm{P}}$, where $0 < \rho < 1$, see Figure 2). Note that *Becker and Shapiro* [2000] used $\varepsilon = \rho/(1-\rho)$ to represent recirculation, but for the formulations here, the parameter ρ is more convenient. Figure 4 illustrates how, because of the presence of a natural flow field, not all tracer mass is expected to be recirculated. In this example, two particles released by the injection well are lost to the flow field so $\rho = 7/8$.

[26] While tracer mass extracted from the pumping well is clearly flux-averaged, the radar measures a resident (volume-averaged) concentration. The amplitude of the radar wave registered at the receiver is a function of the contrast between the electromagnetic properties of the untraced rock matrix and the traced fluid in the fracture [*Tsoflias and Becker*, 2008]. The EM pulse emitted by the radar dipole antennae is effectively a spherically expanding wave front that is reflected from a finite area of the fracture plane. This "illuminated" area of the fracture contributing significant energy to the reflected signal is referred to as the first Fresnel zone, and it is calculated as [*Sheriff and Geldart*, 1995, p. 154]

$$R_{\mathrm{Fr}} = \sqrt{\frac{\lambda d}{2}}, \tag{3}$$

where d is the one-way travel distance and λ is the wavelength of the signal. For 50 MHz antennae and a dielectric constant of 7, wavelength is approximately $\lambda = 2.27$ m. The depth of the fracture is 7.6 m, which gives a radius of the Fresnel zone of 2.9 m. We expect that tracer near the edge of R_{Fr} will have smaller contribution to the reflected signal amplitude than tracer near the center of R_{Fr}, but for this treatment, we consider all returns equivalent. With respect to tracer concentration, this implies that the tracer mass within the Fresnel zone is perfectly mixed.

[27] The application of a resident concentration at a particular location to a flux-averaged concentration measured from a pumping well requires the assumption that our GPR calibration curve was measured at a representative location. In other words, we must assume that stationarity holds and we could have chosen any other location within the tracer flow field to obtain the calibration curve (Figure 5b). As we have stated, this is likely not the case due to expectation that flow channel geometry and fluid salinity are spatially variable. This variability is likely to occur at integral scales on the order of the expected zone of radar illumination. It is unlikely that the fixed-position GPR employed in this experiment images an area of sufficient size to sample a statistical range of concentrations with respect to the statistical range sampled by the migrating tracer. This problem of stationarity is not unique to our experiments, however, because a tracer source domain larger than the integral scale of velocity variations is required for tracer breakthrough at one location to be representative of another location [*Tiedeman and Hsieh*, 2004]. Consequently, we adopt here the assumption of stationarity out of necessity as is customary in the analysis field of tracer tests [*Ginn*, 2002].

[28] The resident concentration for a differential element is related to the flux-averaged concentration by [*Kreft and Zuber*, 1978]

$$C_{\mathrm{R}}(t) = -U\int_0^t \frac{\partial C_{\mathrm{F}}}{\partial x}\mathrm{d}t', \tag{4}$$

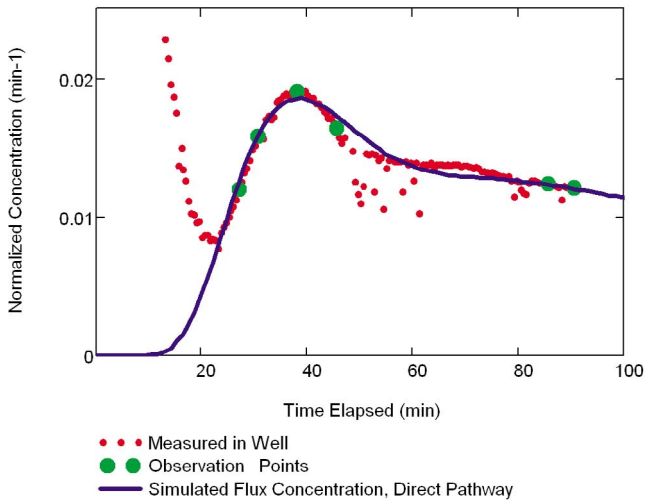

Figure 6. Breakthrough of saline tracer measured at the injection well and best fit simulated breakthrough of most direct single pathway. Fitting is based upon nonlinear regression of selected observation points, and fitted model parameters are shown in Table 1.

where C_F is the flux-averaged concentration and U is the average linear velocity of the fluid. In the present situation, the averaging element has a finite rather than infinitesimal size. This averaging element is taken here to be the Fresnel zone (equation (3)).

[29] We consider tracer storage in the Fresnel zone through simple mass balance. The rate of tracer entering and leaving the Fresnel zone is given by (1) to be

$$\overline{F}_{\text{in}}(s) = \exp\left[\frac{Pe}{2}\left(1 - \sqrt{1 + \frac{4\,\tau_{\text{in}} s}{Pe}}\right)\right] \tag{5}$$

and

$$\overline{F}_{\text{out}}(s) = \exp\left[\frac{Pe}{2}\left(1 - \sqrt{1 + \frac{4\,\tau_{\text{out}} s}{Pe}}\right)\right], \tag{6}$$

respectively. The residence times τ_{in}, τ_{out} are the times at which the tracer enters and departs the Fresnel zone, respectively. If we substitute $\partial x = U\Delta\tau$, where $\Delta\tau = \tau_{\text{out}} - \tau_{\text{in}}$ and account for the integration over time using the identity in Laplace space, equation (4) is computed in the Laplace domain as

$$\overline{C}_{\text{R}}(s) = \frac{M_0}{s\Delta\tau}\left(\overline{F}_{\text{in}} - \overline{F}_{\text{out}}\right). \tag{7}$$

Accounting for reinjection of the tracer into the injection well results in

$$\overline{C}_{\text{R}}(s) = \frac{M_0}{s\Delta\tau}\left(\frac{\overline{F}_{\text{in}} - \overline{F}_{\text{out}}}{1 - \rho\overline{F}_{\text{S}}\overline{F}_{\text{F}}}\right), \tag{8}$$

where $\overline{C}_{\text{R}}(s)$ is the resident concentration as calculated in the Laplace domain.

[30] The time-varying flux-averaged (2) and resident (8) concentrations are calculated by numerically inverting the Laplace solution to the time domain as described above. These functions are fitted to observed data using a Levenberg-Marquardt nonlinear regression formulation [*Matott*, 2008] by comparing predicted and measured breakthrough at selected observation points within the breakthrough curve (indicated in Figures 6 and 7).

4. Results

[31] Recognizing that the streamlines depicted in Figure 4 are contrary to the channelized flow expected in rock fractures and that the true channel geometry is unknown, we consider bounding cases that represent the continuum between completely homogeneous flow and perfectly heterogeneous flow. In the first case, we consider the 14 captured streamlines shown in Figure 4 to be completely dispersed as predicted by a perfect dipole in a weak background flow field (to the southeast). In the second case, we assume that the heterogeneity of the transmissivity field is so severe, such that fluid channels along a single pathway between the injection and pumping well. The reality, we think, is somewhere in between, as has also been conjectured by others [*Tsang and Neretnieks*, 1998].

4.1. All Pathways, Breakthrough at Well

[32] In the perfect dipole scenario, transport was modeled along all pathways predicted in the dipole. The aperture was assumed everywhere constant and equal to the hydraulic aperture derived from cross-hole pumping tests conducted between the injection and pumping well and interpreted using the cubic law [*Snow*, 1965]. The transmissivity T was measured to be 3.2 m^2/d using a Theis analysis of drawdown in well 204 in response from pumping in 304. The cubic law then suggests

$$b = \sqrt[3]{\frac{12\mu T}{\gamma}}, \tag{9}$$

where μ is the dynamic viscosity and γ is the specific weight of water, so that the hydraulic aperture b = 0.38 mm at the ambient water temperature of 12 degrees C.

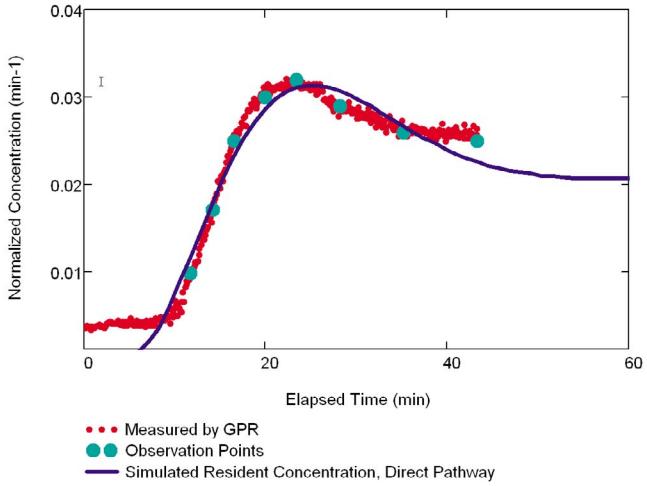

Figure 7. Breakthrough of saline tracer measured by the GPR and best simulated breakthrough based upon nonlinear regression of selected observation points. Fitted parameters shown in Table 2.

Table 1. Fitted Model Parameters and 95% Confidence Upper and Lower Bounds for Flux-Averaged Concentration Measured at Well[a]

Parameter	Optimal Value	Lower Bound	Upper Bound
ρ	0.77	0.72	0.80
α_L (m)	1.4	1.0	1.8
b_{eff} (mm)	0.60	.60	.64

[a]Objective function: 1.1×10^{-6}.

[33] The measured breakthrough at well 304 of saline tracer is shown in Figure 6. Note that the concentration is measured in the injection borehole, so that the first pulse of concentration (0–20 min) is the initial injection and the second is the return due to reinjection of the pumped water. The first pulse is used independently to determine the borehole volume assuming a perfectly mixed tank, which results in an exponentially decaying transfer function. The effective borehole volume was determined to be 11.4 L by fitting the initial concentration decrease in the borehole. Tracer breakthrough showed a slight increase (hump) in concentration at about 70 min into the test because of an unanticipated fluctuation in the water flow from the surface tank to the borehole.

[34] Selected observation points along the breakthrough curve (Figure 6) were used to fit the theoretical model to the measured breakthrough. These points were selected to avoid the concentration hump because of the temporary increase in tank discharge but provide an even weighting of representative concentrations elsewhere. The fitted parameters were ρ, α_L, and the effective mean aperture b_{eff}. The effective mean aperture accounts for the well-known difference in tracer and hydraulic aperture [*Tsang*, 1992]. Calibration of b_{eff} was accomplished by scaling the effective porosity in the particle tracking algorithm. Making these assumptions, it was not possible to find a reasonable match between the full dipole model and the measured tracer breakthrough. The best fit using nonlinear regression produced a peak concentration that was only 70% of the measured concentration. The poor representation of breakthrough occurs because the longest streamlines carry a significant fraction of the tracer mass (Figure 4), transferring much of the tracer mass to very late time breakthrough. This late time arrival of tracer is not observed in the experimental breakthrough curve. Consequently, we can discard the full-dipole model as a viable explanation for our field data.

4.2. Most Direct Pathway, Breakthrough at Well

[35] In the direct breakthrough scenario, all tracer moves along the most direct pathway between injection and pumping wells (Figure 4). This direct pathway is traced as before, along a particle path predicted by the idealized flow field. Although one pathway is considered, the variable transport velocity is still predicted by the idealized (homogeneous T) dipole hydraulic field. The tracking particle was located at the injection well, on a straight line that connects the injection and pumping wells. Under this bounding scenario, a much better fit is achieved. The parameters optimized through linear regression are shown in Table 1, and the simulated breakthrough are shown in Figure 6. The optimization indicates that 77% of the traced water was recirculated to the injection well (ρ = 0.77). Incomplete recirculation is likely due to the influence of the cross-flow from the natural groundwater gradient at the site. The fitted effective aperture of 0.60 mm is somewhat larger than the hydraulic aperture of 0.38 mm determined from the hydraulic connection between the two wells but closer to the average hydraulic aperture of 0.45 mm determined from Theis analysis cross-hole pump tests conducted among six available boreholes at the locale [*Talley et al.*, 2005]. The fitted longitudinal dispersivity is 1.4 m, suggesting Pe = 10, when the 14 m distance between the injection and pumping wells is taken as a characteristic length.

4.3. Direct Pathway, Measured by Radar

[36] We model breakthrough measured by the calibrated radar using the resident concentration formulation of transport. The resident-concentration transport model (8) was calibrated to the radar-measured breakthrough using two fitting parameters: α_L and b_{eff}. The recirculation parameter ρ was assumed to be 0.77 as determined from the flux-averaged breakthrough fitting. The rationale for assuming rather than fitting ρ is that the flux-averaged concentration should be more sensitive to recirculation than the resident concentration. The radar detects only the portion of the tracer breakthrough within the Fresnel zone, whereas the concentration in the boreholes is affected by all transport pathways.

[37] The model provided an adequate fit of the breakthrough data (Figure 7). The optimized parameters (Table 2) are similar to the parameters determined through the fitting of the flux-averaged concentration. The optimized longitudinal dispersivity is identical to that determined from flux-averaged concentration (Pe = 10), and the estimated effective aperture (0.45 mm) is slightly smaller than that determined from the flux-averaged concentration (0.60 mm). This aperture estimate is identical to the averaged aperture measured from Theis analysis of drawdown among all wells in the field.

4.4. Summary of Model Result

[38] The findings of the modeling study can be summarized as follows:

[39] 1. The classic full-dipole (doublet) flow field is an inappropriate model for recirculated flow between the two test wells. This conclusion is obtained from the short tracer breakthrough times and confirmed through an accounting of tracer mass passing beneath the radar.

[40] 2. A single direct streamline model provides a satisfactory estimate of flux-averaged concentration measured at the breakthrough well.

[41] 3. The direct streamline model also provides a satisfactory estimate of resident concentration measured by the radar.

[42] 4. The appropriate transport models fitted to the flux and resident concentrations produce identical estimates of

Table 2. Fitted Model Parameters and 95% Confidence Upper and Lower Bounds for Resident Concentration Measured by GPR[a]

Parameter	Optimal Value	Lower Bound	Upper Bound
α_L (m)	1.4	1.1	1.7
b_{eff} (mm)	0.45	0.41	0.49

[a]Objective function = 2.0×10^{-5}.

dispersivity and similar estimates (within 25%) of effective aperture.

[43] 5. Effective apertures estimated from flux and resident tracer breakthrough agree favorably (within 25%) to average hydraulic aperture derived from Theis analysis of cross-hole pump tests.

5. Discussion

[44] Current understanding of transport of dissolved mass in bedrock groundwater comes primarily from tracer tests and the interpretation of breakthrough curves. Breakthrough curves represent an averaging through time of all pathways of the tracer from the injection to the pumping well, so inverting the breakthrough curve to derive transport parameters is a highly nonunique process. Alternative mathematical models may achieve acceptable results. We use here the traditional advection-dispersion equation formulated as a first-passage-time problem. The advection-dispersion equation in its classic form has endured much criticism as of late, and many promising alternatives have been proposed. We do not enter into this discussion here. Rather, we consider the advection-dispersion equation as a convenient benchmark and focus on adding more useful data to the discussion.

[45] The exact geometry of hydraulic pathways that connect the injection and pumping well is not known so we use here two bounding cases: (1) a theoretical dipole in which a large area is swept by the tracer and (2) a direct one-dimensional path in which a relatively small area is swept by the tracer. A common method of determining "swept area" of a tracer is to use the mean tracer residence time in the formation and the pumping rate:

$$A = \frac{Q_p \tau}{b_{\text{eff}}}, \tag{10}$$

where τ is the mean residence time determined from the first moment of the breakthrough curve. Normally, one finds the mean residence time τ by calculating the first moment of the tracer breakthrough directly. This is complicated in our tests by the recirculation of fluid and by the residence time in the wellbore and tracer reservoir. Instead, we find the simple mean residence time by fitting (1) to the breakthrough, accounting for reinjection using (8), which amounts to assuming that tracer is distributed as an inverse Gaussian probability density function [*Becker and Charbeneau*, 2000]. Fitting the model to breakthrough produces τ = 44 min, so substituting b_{eff} = 0.38 mm (from the hydraulic tests) and Q_p = 2.8 L/min (measured) results in the swept area, A = 324 m^2. This is the approximate half of the area swept by the captured particles as shown in Figure 4. Thus, we think that only about half the fracture is conducting fluid and tracer in an efficient manner.

[46] Although the swept area found from equation (10) reasonably approaches that predicted by the particle tracking, the arrival times suggest that all travel paths are not equally viable. The mean arrival time of 325 min predicted from the particle tracking shown in Figure 4 is far greater than the observed or modeled mean residence time of the tracer. The large theoretical arrival time comes primarily from the more circuitous paths traced by particles on the west side of the injection well. If one accounts for only the particle paths that travel within the well field (i.e., the shortest nine paths), the average residence time becomes 44 min that approximates the mean breakthrough arrival. These central paths account for about one third of the total area swept by the captured particles or about two thirds of the swept area predicted by equation (10). Simulations that constrain transport to only these paths, however, do not produce a significantly better representation of the tracer breakthrough curve than the single direct pathway. This suggests that the central pathways connecting the two wells do not have markedly different velocities. Such behavior would be expected under the assumption of highly channelized flow, where flow is less impacted by the divergent and convergent flow fields near the wells [*Tsang and Neretnieks*, 1998]. Flow is better represented under these conditions by conceptual "streamtubes" with diameters that do not vary greatly with the distance from the wells. A similar result was obtained for two-well tracer tests conducted in a fractured crystalline bedrock [*Becker and Shapiro*, 2000].

[47] An interpretation of highly channelized flow appears also to be supported by the radar information. According to our mass balance analysis, nearly all of the injected saline mass passes beneath the view of the radar. The radar view is considered here to be approximately equivalent to the first Fresnel zone (equation (3)) that has a radius of 2.9 m (Figure 4). Indeed, the central particle tracking paths do pass through or near to the Fresnel zone, but we emphasize that the Fresnel zone is only an approximation of the area of the fracture that reflects radar energy to the receiving antenna.

[48] The difference between flux-averaged and resident concentrations is significant in these tests. To illustrate this difference, we calculate a one-dimensional transfer function for flux-averaged (1) and resident (7) concentration, removing the complicating influences of delayed source term and recirculation. The flux-averaged concentration is calculated for tracer that passes a control plane located in the center of the Fresnel zone. The source term is considered to be a Dirac pulse to simplify the discussion. In the first example, we collapse the Fresnel zone to a 10 cm diameter to remove the effect of area averaging. We compare flux-averaged and resident concentrations in a case where the Peclet number (Pe) is assumed to be 10 (as estimated from our tests) and another where Pe = 100. Flux-averaged and resident concentrations are dissimilar in the case of Pe = 10 (large longitudinal dispersivity) but are indistinguishable in the case of Pe = 100 (small longitudinal dispersivity). It seems quite reasonable, therefore, to disregard the difference between flux-averaged and resident concentration in cases where the dispersivity is small in comparison with transport distances (e.g., homogeneous porous media) but not where dispersivity comes within an order-of-magnitude of transport distance (e.g., heterogeneous fractured bedrock such as at Altona).

[49] Also shown in Figure 8 is a theoretical case in which the Fresnel zone has not been collapsed but is retained at the diameter estimated in these experiments. The flux-averaged concentration is unaffected by this change as it is calculated at a control plane. It is apparent that the size of the Fresnel zone has a large impact on resident concentrations at high Pe but very little impact at low Pe. Thus, longitudinal dispersivity seems to overcome the influence of averaging within the Fresnel zone at low Pe. As a consequence, although we do not expect our estimate of the Fresnel zone

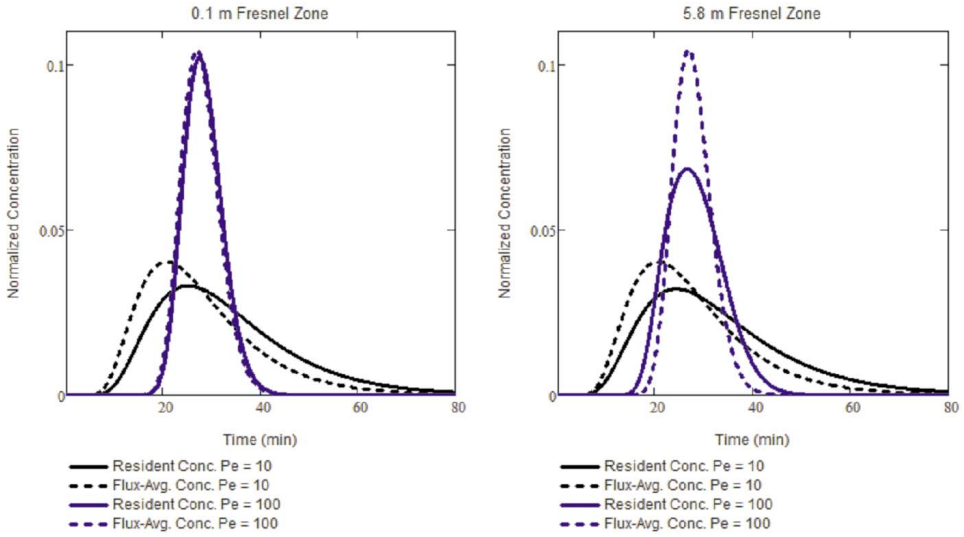

Figure 8. Theoretical breakthrough curves measured as resident and flux-averaged concentration under different conditions of dispersivity (Peclet number) and diameter of the Fresnel zone.

from equation (3) to be rigorous, uncertainty in the size of the Fresnel zone should have little influence on our analysis of transport.

[50] Although the inversion of the tracer curves using the assumed model was mathematically conclusive, it was not entirely satisfying. In particular, the resident concentration model did not capture all of the qualities of the breakthrough of tracer under the radar. This may be due to the nonsynchronous arrival of multiple pathways within the view of the radar. In fact, such behavior is expected based upon the analysis of the flow field using both hydraulic and tracer information. At this moment, it is not known how the radar averages concentrations within its view because the aperture field is unknown. Some weighting based upon concentration and aperture is suggested by the theoretical reflection coefficient model. Three-dimensional numerical simulations are necessary to assess how channeled saline flow through a fracture is imaged by a distant radar at the surface. We are in the process of conducting such modeling studies to address these questions of the effect of spatial heterogeneity to reflected GPR signals.

6. Conclusions

[51] We used tracer experiments in fractured bedrock to investigate the difference in flux-averaged versus resident concentrations in highly heterogeneous flow systems. Flux-averaged concentrations were measured by sampling pumped water and resident concentrations were derived from reflected GPR amplitudes measured at the surface. Table salt was used as a tracer in a single subhorizontal bedding plane fracture. Saline concentrations were derived from radar reflected amplitudes by first calibrating the radar to controlled concentrations within the fracture.

[52] The GPR produced measures of saline concentration in the fracture that were sufficiently reliable to produce a complete tracer breakthrough curve. We emphasize, however, that reflected radar amplitude is a function of both electrical conductivity and fracture aperture [*Tsoflias and Becker*, 2008]. We were able to derive saline tracer concentrations by experimentally calibrating the reflected signal amplitudes to saline concentration at the same position in which the breakthrough was measured. This calibration curve is not immediately applicable to GPR reflections at other locations in the well field. We note, however, that the GPR methods presented here are applicable to other fractured bedrock sites.

[53] The forced-gradient tracer experiment was conducted in full-dipole mode, meaning that all pumped water was returned to the injection well. The recirculation of traced water complicated analysis but was deemed necessary to prevent simultaneous alteration of the flow field and tracer concentration (e.g., as is the case with tracer slug injection). Recirculation of traced water was taken into account using transfer function models employing a first-passage-time formulation of the advection-dispersion equation. A new transfer function representation of resident concentration was developed to correctly account for the imaging of saline tracer by the radar, which amounts to a resident rather than flux-averaged measurement of tracer mass.

[54] Analysis of tracer breakthrough at the well suggests that the theoretical dipole flow field in a homogeneous conductivity field is not an appropriate model for this system. The more circuitous pathways predict tracer arrival times far greater than those observed at the pumping well. In fact, tracer arrival at the well was better represented by a single direct flow path or a number of more direct flow paths that connect the injection and pumping wells. This conceptual model was confirmed by analysis of the radar breakthrough, which indicates nearly all tracer mass passed within view of the radar antennae that were placed directly between the pumping and injection wells.

[55] The flux-averaged concentration model of the tracer breakthrough at the well and the resident concentration model of tracer presence beneath the radar, adequately depict the breakthrough curves. A nonlinear regression showed a narrow 95% confidence interval about the fitted parameters. Modeling of the flux-averaged tracer arrival at the well indicates that 77% of the tracer was recirculated from pumping to injection well, with the remainder lost to

the background flow field that crosses obliquely the induced hydraulic field. An ideal dipole field interacting with the measured background flow field would be expected to lose 87% of the tracer during recirculation.

[56] Longitudinal dispersivity produced by the optimization procedure was exactly the same for the flux-averaged tracer measured at the well and the resident concentration measured by the radar. The effective aperture extracted from the radar amplitudes (0.45 mm) was smaller than that extracted from the well concentrations (0.60 mm), but both were slightly larger than that determined using the cubic law and Theis drawdown analysis between the same two wells (0.38 mm). The effective aperture estimated from the radar breakthrough was, perhaps coincidentally, exactly the same as the aperture estimated from pump tests in the same well field [*Talley et al.*, 2005].

[57] When longitudinal dispersivity is small compared to overall transport length (large Peclet numbers), there appears to be little difference between the flux-averaged and resident concentration. In cases where dispersivity approaches transport distance (small Peclet numbers), such as at this experimental site, the difference between flux-averaged and resident concentrations becomes significant. For these experiments, therefore, making a theoretical distinction between flux-averaged versus resident concentrations can be important for correct interpretation of solute transport in groundwater.

[58] As subsurface geophysical imaging continues to improve, more field measurements of resident solute concentrations will become available. Our findings suggest that, in highly heterogeneous flow fields, interpretation of these data will benefit from joint analysis of resident concentration and flux-based measurements at monitoring wells. We consider here only nonreactive transport. Resident concentrations will prove to be more valuable in studies of reactive transport where local concentration dominates transformation and adsorption of contaminants.

[59] **Acknowledgments.** The authors are grateful for the continuing support provided by David Franzi and Edwin Romanowicz at SUNY Plattsburgh and the William H. Miner Agricultural Research Institute. Renee Bourque, Jeremy Crowley, and Greg Babonis provided tireless help in the field. The thoughtful comments of the three anonymous reviewers much improved the clarity of the discussion and are greatly appreciated. These findings are based in part upon work supported by the National Science Foundation under grant GEO-0207720 and ITR-0426557 and the American Chemical Society PRF 43401-G8. Acquisition of the GPR system was funded by the National Science Foundation EAR/IF-0345445. Any opinions, findings, and conclusions or recommendations expressed in this material are those of the author(s) and do not necessarily reflect the views of the National Science Foundation.

References

Aris, R. (1956), On the dispersion of a solute in a fluid flowing through a tube, *Proc. R. Soc. London Ser. A.*, *235*, 66–77.

Balanis, C. (1989), *Advanced Engineering Electromagnetics*, 220–236 pp., John Wiley and Sons, Inc., New York.

Becker, M. W., and R. J. Charbeneau (2000), First-passage-time transfer functions for groundwater tracer tests conducted in radially convergent flow, *J. Contam. Hydrol.*, *45*, 361–372.

Becker, M. W., and A. M. Shapiro (2000), Tracer transport in fractured crystalline rock; evidence of nondiffusive breakthrough tailing, *Water Resour. Res.*, *36*, 1677–1686, doi:10.1029/2000WR900080.

Becker, M. W., and A. M. Shapiro (2003), Interpreting tracer breakthrough tailing from different forced-gradient tracer experiment configurations in fractured bedrock, *Water Resour. Res.*, *39*(1), 1024, doi:10.1029/2001WR001190.

Becker, M. W., and Z. Jiang (2007), Flux-based contaminant transport in a GIS environment, *J. Hydrol.*, *343*, 203–210.

Bourke, P. J. (1987), Channeling of flow through fractures in rock, paper presented at GEOVAL-87 International Symposium, Swed. Nucl. Power Insp (SKI), Stockholm, Sweden, 7–9 April 1987.

Dankwerts, P. V. (1953), Continuous flow systems (distribution of residence times), *Chem. Eng. Sci.*, *2*, 1–13.

Davis, J. L., and A. P. Annan (1989), Ground penetrating radar for high resolution mapping of soil and rock stratigraphy, *Geophys. Prospect.*, *37*, 531–551.

Day-Lewis, F. D., et al. (2003), Time-lapse imaging of saline-tracer transport in fractured rock using difference-attenuation radar tomography, *Water Resour. Res.*, *39*(10), 1290, doi:10.1029/2002WR001722.

Day-Lewis, F. D., et al. (2006), Combined interpretation of radar, hydraulic, and tracer data from a fractured-rock aquifer near Mirror Lake, New Hampshire, USA, *Hydrogeol. J.*, *14*, 1–14.

Ginn, T. R. (2002), Streamtube ensemble techniques for subsurface multicomponent reactive transport, in *Stochastic Methods in Subsurface Contaminant Hydrology*, edited by R. S. Govindaraju, Am. Soc. Civ. Eng., Washington, D.C.

Grasmueck, M. (1996), 3-D ground-penetrating radar applied to fracture imaging in gneiss, *Geophysics, 61*, 1050–1064.

Gregoire, C., and F. Hollender (2004), Discontinuity characterization by the inversion of the spectral content of ground-penetrating radar (GPR) reflections—Application of the Jonscher model, *Geophysics*, *69*, 1414–1424.

Gregoire, C., et al. (2003), GPR abilities for the detection and characterization of open fractures in a salt mine, *Near Surface Geophysics*, *1*, 139–147.

Gregoire, C., et al. (2006), Use of borehole radar reflection logging to monitor steam-enhanced remediation in fractured limestone—Results of numerical modelling and a field experiment, *J. Appl. Geophys.*, *60*, 41–54.

Hubbard, S. S., and Y. Rubin (2000), Hydrogeological parameter estimation using geophysical data: a review of selected techniques, *J. Contam. Hydrol.*, *45*, 3–34.

Kreft, A., and A. Zuber (1978), Physical meaning of dispersion-equation and its solutions for different initial and boundary conditions, *Chem. Eng. Sci.*, *33*, 1471–1480.

Lane, J. W., Jr., et al. (2000), Evaluation of ground-penetrating radar to detect free-phase hydrocarbons in fractured rocks—Results of numerical modeling and physical experiments, *Ground Water*, *38*, 929–938.

Liu, H. H., et al. (2007), An interpretation of potential scale dependence of the effective matrix diffusion coefficient, *J. Contam. Hydrol.*, *90*, 41–57.

Matott, L. S. (2008), OSTRICH: An Optimization Software Tool; Documentation and User's Guide (Version 1.6), Dep. of Civ., Struct. Environ. Eng., Univ. at Buffalo, SUNY, Buffalo, NY.

Moreno, L., et al. (1985), Analysis of some laboratory tracer runs in natural fissures, *Water Resour. Res.*, *21*, 951–958, doi:10.1029/WR021i007p00951.

Muldoon, M., and K. Bradbury (2005), Site characterization in density fractured dolomite: Comparison of methods, *Ground Water*, *43*(6), 863–876.

Neretnieks, I., et al. (1982), Tracer movement in a single fissure in granitic rock: Some experimental results and their interpretation, *Water Resour. Res.*, *18*, 849–858, doi:10.1029/WR018i004p00849.

Neretnieks, I. (1983), A note on fracture flow dispersion mechanisms in the ground, *Water Resour. Res.*, *19*, 364–370.

Neretnieks, I. (1987), Channeling effects in flow and transport in fractured rocks—Some recent observations and models, paper presented at GEOVAL-87 International Symposium, Swed. Nucl. Power Insp. (SKI), Stockholm.

Rabideau, A. J., et al. (2007), Analytic-element modeling of supraregional groundwater flow: Concepts and tools for automated model configuration, *J. Hydrol. Eng.*, *12*, 83–96.

Rayburn, J. A., et al. (2005), A series of large, Late Wisconsinan meltwater floods through the Champlain and Hudson Valleys, New York State, USA, *Quat. Sci. Rev.*, *24*, 2410–2419.

Seol, S. J., et al. (2001), Finding the strike direction of fractures using GPR, *Geophys. Prospect.*, *49*, 300–308.

Shapiro, A. M. (2001), Effective matrix diffusion in kilometer-scale transport in fractured crystalline rock, *Water Resour. Res.*, *37*(3), 507–522, doi:10.1029/2000WR900301.

Shapiro, A. M., and V. D. Cvetkovic (1988), Stochastic-analysis of solute arrival time in heterogeneous porous-media, *Water Resour. Res.*, *24*, 1711–1718, doi:10.1029/WR024i010p01711.

Sheriff, R. E., and L. P. Geldart (1995), *Exploration Seismology*, 2nd ed., Cambridge Univ. Press.

Snow, D. T. (1965), A parallel plate model of fractured permeabile media, Ph.D. thesis, Univ. of Calif., Berkley.

Stephenson, K. M., and K. S. Novakowski (2006), The analysis of pulse interference tests conducted in a fractured rock aquifer bounded by a constant free surface, *J. Hydrol.*, *319*, 109–122.

Talley, J. (2005), Imaging channelized flow in fractured rock using surface GPR, M.S. thesis, Univ. at Buffalo, Buffalo, NY.

Talley, J., et al. (2005), Four-dimensional mapping of tracer channelization in subhorizontal bedrock fractures using surface ground penetrating radar, *Geophys. Res. Lett.*, *32*, L04401, doi:10.1029/2004GL021974.

Tiedeman, C. R., and P. A. Hsieh (2004), Evaluation of longitudinal dispersivity estimates from simulated forced- and natural-gradient tracer tests in heterogeneous aquifers, *Water Resour. Res.*, *40*, W01512, doi:10.1029/2003WR002401.

Tsang, C. F., and I. Neretnieks (1998), Flow channeling in heterogeneous fractured rocks, *Rev. Geophys.*, *36*, 275–298.

Tsang, Y. W. (1992), Usage of "equivalent apertures" for rock fractures as derived from hydraulic and tracer tests, *Water Resour. Res.*, *28*, 1451–1455, doi:10.1029/92WR00361.

Tsoflias, G. P. (2008), GPR imaging of dual porosity rocks, *The Leading Edge*, *27*, 1436–1445.

Tsoflias, G. P., and M. W. Becker (2008), Ground-penetrating-radar response to fracture-fluid salinity: Why lower frequencies are favorable for resolving salinity changes, *Geophysics*, *73*, J25–J30.

Tsoflias, G. P., et al. (2001), Monitoring pumping test response in a fractured aquifer using ground-penetrating radar, *Water Resour. Res.*, *37*(5), 1221–1229, doi:10.1029/2000WR900297.

Zhou, Q. L., et al. (2007), Field-scale effective matrix diffusion coefficient for fractured rock: Results from literature survey, *J. Contam. Hydrol.*, *93*, 161–187.

M. W. Becker, California State University, 1250 Bellflower Blvd., Long Beach, CA 90840, USA. (mbecker3@csulb.edu)

G. P. Tsoflias, University of Kansas, 1475 Jayhawk Blvd., Lawrence, KS 66045, USA. (tsoflias@ku.edu)